

## ROTATIONAL LINE EMISSION FROM WATER IN PROTOPLANETARY DISKS

R. MEIJERINK<sup>1</sup>, D.R. POELMAN<sup>2</sup>, M. SPAANS<sup>3</sup>, A.G.G.M. TIELENS<sup>4,3</sup>, AND A.E. GLASSGOLD<sup>1</sup>

*Draft version November 6, 2018*

### ABSTRACT

Circumstellar disks provide the material reservoir for the growth of young stars and for planet formation. We combine a high-level radiative transfer program with a thermal-chemical model of a typical T Tauri star disk to investigate the diagnostic potential of the far-infrared lines of water for probing disk structure. We discuss the observability of pure rotational H<sub>2</sub>O lines with the *Herschel Space Observatory*, specifically the residual gas where water is mainly frozen out. We find that measuring both the line profile of the ground 1<sub>10</sub> – 1<sub>01</sub> ortho-H<sub>2</sub>O transition and the ratio of this line to the 3<sub>12</sub> – 3<sub>03</sub> and 2<sub>21</sub> – 2<sub>12</sub> line can provide information on the gas phase water between 5-100 AU, but not on the snow line which is expected to occur at smaller radii.

*Subject headings:* accretion, accretion disks – infrared: stars – planetary systems: protoplanetary disks – stars: formation: pre-main sequence – X-rays: stars – radiative transfer

### 1. INTRODUCTION

The radius where volatiles sublimate in a protoplanetary disk plays an important role in planet formation. One volatile of particular interest is water, and the place where it sublimates or freezes out onto grains is called the *snow line* (Hayashi 1981). The sublimation temperature for water ranges from  $T \sim 110$ – $170$  K, depending on the water vapor pressure (cf. Fraser et al. 2001; Podolak & Zucker 2004). At radii larger than the snow line, it is possible to hydrate planetesimals and protoplanets. Hayashi (1981) found that the snow line is now located at about 2.7 AU from the Sun in our own Solar System. However, the position can be different for a T Tauri star. Its location depends on the evolutionary phase of the disk, and it can vary from 0.7 to 10 AU (Sasselov & Lecar 2000; Lecar et al. 2006; Garaud & Lin 2007).

Gas phase water is expected to be abundant between the water-ice sublimation temperature  $T \sim 110$ – $170$  K and the dissociation temperature  $T \sim 2500$  K. Its rich spectrum covers almost all astronomically available wavelength bands. Using the near-infrared lines near  $2.3\mu\text{m}$ , Carr et al. (2004) and Thi & Bik (2005) found warm H<sub>2</sub>O in protoplanetary disks at temperatures  $T > 1200$  K and radii  $R < 0.4$  AU, and Carr & Najita (2008) and Salyk et al. (2008) have detected mid-infrared water lines with *Spitzer*. The far-infrared spectrometers aboard the *Herschel* space telescope will offer the opportunity to measure the pure rotational transitions of this important molecule, which are characteristic of gas temperatures of  $T \gtrsim 60$  K. Because gas phase H<sub>2</sub>O requires warm conditions ( $T \gtrsim 200$  K) it is expected to be abundant at small radii and thus perhaps not observable with the *Herschel* spectrometers. However, temperatures appropriate to both the occurrence and detection of H<sub>2</sub>O

are present over a wide range of radii because stellar radiation heats the disk atmosphere. Moreover, as we show in this letter, several lines of H<sub>2</sub>O can be detected by *Herschel* at very low abundances close to the mid-plane where the bulk of the water is frozen. The detection of these lines will complement the previous measurements of the near-infrared and mid-infrared water lines.

### 2. MODELS

The calculation is done as follows: (1) We use an X-ray irradiated disk code to calculate the temperature structure and molecular abundances for a generic T Tauri disk. (2) The results are input into a multi-zone radiative transfer code that includes the calculation of the excitation of the H<sub>2</sub>O lines. (3) A ray-tracing code is used to obtain line fluxes and line shapes. These three steps are discussed in more detail below.

#### 2.1. The thermal and chemical structure of the disk

The thermal-chemical structure of the disk is calculated with the code described by Glassgold et al. (2004) with minor corrections and updates (Meijerink et al. 2008). The disk is illuminated by stellar X-rays with a thermal spectrum with temperature  $T_X = 1$  keV and luminosity  $L_X = 2 \times 10^{30}$  erg s<sup>-1</sup>. In regions where the X-rays are strongly attenuated, the disk is ionized by the decay products of <sup>26</sup>Al at a rate  $\zeta_{26} = 4 \times 10^{-19}$  s<sup>-1</sup>. The density structure is given by the generic T Tauri disk model (Paola d’Alessio, private communication) with accretion rate  $\dot{M} = 10^{-8} M_\odot \text{yr}^{-1}$  and stellar parameters  $M_* = 0.5 M_\odot$ ,  $R_* = 2R_\odot$ , and  $T_* = 4000$  K. The disk is flared, and the density varies continuously from  $R = 0.028$  to  $>500$  AU. The model density does not include modifications such as holes, gaps, and rims suggested, for example, by the spectral energy distributions measured with *Spitzer* (e.g., Dullemond et al. 2007). The adopted model has a power law grain size distribution with index  $p = -3.5$  and minimum and maximum grain sizes of  $a_{min} = 0.005$  and  $a_{max} = 1000 \mu\text{m}$ , respectively, resulting in a geometric mean grain size,  $a_g = 2.24 \mu\text{m}$ . The grain size  $a_g$  determines the thermal coupling between dust and gas.

Electronic address: rowin@astro.berkeley.edu

<sup>1</sup> Astronomy Department, University of California, Berkeley, CA 94720, United States

<sup>2</sup> School of Physics & Astronomy, University of St Andrews, North Haugh, St Andrews KY16 9SS, Scotland

<sup>3</sup> Kapteyn Astronomical Institute, P.O. Box 800, 9700 AV Groningen, The Netherlands

<sup>4</sup> NASA Ames Research Center, MS245-3, Moffett Field, CA 94035, USA

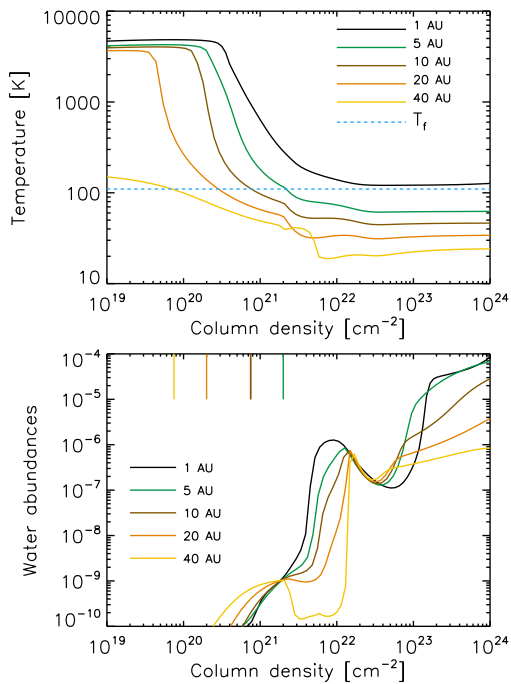


FIG. 1.— Temperature (top), and fractional water abundance (bottom) vs. perpendicular column density. The dotted blue line (top) shows the freeze-out temperature  $T_f = 110$  K. The colored tick marks at the top of the bottom panel indicate the smallest perpendicular column density for each radius where water freezes out. No freeze-out occurs within  $R = 1$  AU. Note the non-monotone variation of the water abundance due to gradients in the ionization rate, density, and temperature.

The D’Alessio et al. (1999, 2001) dust temperature involves a balance between heating by viscous dissipation, FUV/optical/IR radiation, cosmic rays and cooling by IR radiation. Our gas temperature is determined by heating by penetrating X-rays, gas-grain collisions and cooling by atomic and molecular lines. The gas thermal model relies solely on X-ray irradiation in contrast to UV irradiation models by Jonkheid et al. (2004, 2007), Kamp & Dullemond (2004), and Nomura et al. (2007) (who also include X-rays), who include UV photons. The UV irradiation, however, play no role in the regions where the submillimeter  $\text{H}_2\text{O}$  emission is produced. The numerical approach is “1+1D”, i.e., the vertical thermal and chemical structure is calculated independently at 45 radial points whose spacing increases with radius. However, the X-ray attenuation is calculated along the line-of-sight to the star. The photons can only escape in the vertical direction, a reasonable approximation, since the opacities in the radial direction are so much larger.

The chemistry is steady state and entirely gas phase, and it includes only carbon and oxygen bearing species. It does not treat freeze-out of  $\text{H}_2\text{O}$  in detail, but we expect that freeze-out cannot be 100% efficient. Incomplete freeze-out has been observed by ISO (Boonman et al. 2003), and Davis (2007) has modeled freeze-out in irradiated accretion disks. In order to treat the freeze-out of water, we assume a fixed gas-phase water abundance,  $x_f(\text{H}_2\text{O}) = 10^{-8}$  or  $x_f(\text{H}_2\text{O}) = 10^{-10}$ , in regions where most of the water is expected to freeze-out on grains, i.e., where the gas temperature satisfies the condition  $T < T_f$  with  $T_f = 110$  K, the adopted freeze-out temperature. Where the model gas phase abundance

is lower, we adopt the calculated abundance. A more realistic treatment of water freeze-out would involve treating many poorly understood physical processes beyond the scope of this short report. These might include the growth and settling of the dust grains, molecular synthesis and transformation on grain surfaces, adsorption and desorption, and mixing. We are developing an improved thermal-chemical disk model that will address many of these issues. The advantage of the present model is that it allows us to isolate the chemical effects of freeze-out and the effects of grain growth and settling in a simple albeit preliminary way.

## 2.2. Water radiative transfer

The critical densities of the lines of interest are typically large, in the range  $n_{\text{crit}} \sim 10^8 - 10^{10} \text{ cm}^{-3}$ . The fractional abundance of gaseous water becomes significant at perpendicular column densities  $N_{\text{H}} > 2 - 5 \times 10^{21} \text{ cm}^{-2}$  (Fig.1), and the excitation can be subthermal, especially at large radii ( $R > 10 - 20$  AU). Thus assuming local thermodynamic equilibrium is not always a good approximation, and a full radiation transfer calculation is required.

We calculate the level populations of  $\text{H}_2\text{O}$  using the multi-zone escape probability method  $\beta 3\text{D}$  described by Poelman & Spaans (2005, 2006). We assume Keplerian rotation for a stellar mass  $M_* = 0.5 M_{\odot}$  and turbulent velocities  $\delta v = 0.5$ , and  $2.0 \text{ km s}^{-1}$  (where  $\delta v$  is the  $1/e$  half width of line profile). In the multi-zone formalism, the medium is divided into a large number of grid cells, each with calculated values of the volumetric hydrogen density, the temperatures of gas and dust, and the  $\text{H}_2\text{O}$  abundance. The connection of every grid cell with all the others enables us to solve locally the equations of statistical equilibrium taking into account global information for the entire disk. Radiative and collisional excitation and de-excitation by electrons and atomic and molecular hydrogen, and dust pumping are included, using data from Faure & Josselin (2008) and the Leiden Atomic and Molecular Database (LAMDA, Schöier et al. 2005). We adopt the dust opacities from D’Alessio et al. (2001). Although the radiative transfer code can deal with three dimensions, we only consider 1D slabs as in the thermal-chemical calculation.

## 2.3. Ray tracing

We compute line profiles for inclinations ranging from  $0^\circ$  to  $90^\circ$  with the sky brightness distribution program SKY, which is part of the RATRAN code (Hogerheijde & van der Tak 2000). We use the 2-dimensional cylindrically-symmetric version of SKY, and the resulting level populations, densities and molecular abundances are combined and rebinned into a single grid at each radius. The dynamical ranges of the physical and chemical properties are large in the vertical direction, and we use 400 cells in this direction and decrease the cell size toward the disk midplane. Fewer grid cells are needed in the radial direction since the changes are more gradual, although smaller spacings are also used at small radii.

## 3. RESULTS & DISCUSSION

Fig. 1 shows the gas temperature and  $\text{H}_2\text{O}$  abundance for a range of radii from  $R = 1 - 40$  AU plotted versus in-

creasing perpendicular column density  $N_{\text{H}}$ . As explained in more detail in Glassgold et al. (2004) and Meijerink et al. (2008), the stellar X-rays heat the gas at the top of the atmosphere as high as  $T \sim 3000 - 4000$  K for  $R < 20$  AU. Attenuation of the X-rays for  $N_{\text{H}} > 10^{21} \text{ cm}^{-2}$  produces a drop in temperature and induces transitions from atoms (or ions) to molecules. For example, the H to  $\text{H}_2$  transition occurs for  $N_{\text{H}} = 10^{21} - 10^{22} \text{ cm}^{-2}$ . The water abundance before the H to  $\text{H}_2$  transition is small due to the efficient destruction by X-ray ionized species such as  $\text{H}^+$  and  $\text{He}^+$ . Congruent with the H to  $\text{H}_2$  transition, the water abundance increases steeply.

According to Fig. 1, freeze-out occurs for  $R > 1$  AU and beyond  $N_{\text{H}} \sim 10^{19} - 10^{22} \text{ cm}^{-2}$  depending on the radius (as indicated by the colored tick marks for each radius). The volumetric densities here are quite high,  $n_{\text{H}} = 10^8 - 10^{12} \text{ cm}^{-3}$  and, despite the reduced dust surface area in the thermal-chemical model, the gas is thermally coupled to the dust. At even higher column densities than are shown in Fig. 1 (closer to the mid-plane), the temperature increases slightly due to viscous accretion heating. Temperatures greater than  $T \sim 200$  K are needed for efficient gas phase synthesis of water by neutral radical reactions, and they are only attained at small radii  $R < 0.5$  AU, where  $x_{\text{H}_2\text{O}} > 10^{-4}$  for  $N_{\text{H}} > 10^{22} - 10^{23} \text{ cm}^{-2}$ .

We have calculated line profiles and fluxes for the low-excitation  $\text{H}_2\text{O}$  transitions that are in the spectral range of *Herschel Photodetector Array Camera and Spectrometer* (PACS) and *Heterodyne Instrument on the Far-Infrared* (HIFI). The results indicate that a number lines in the frequency bands of HIFI are detectable. The frequency bands of PACS are less favorable, and the following discussion is based on HIFI. The integrated fluxes are summarized in Table 1 for sources at an assumed distance of 140 pc. During the first *Herschel* observation cycle, only the ortho  $1_{10} - 1_{01}$  and para  $1_{11} - 0_{00}$  ground level transitions will be observed in the *Herschel* key program "Water in Star-forming Regions With *Herschel*" (<http://www.strw.leidenuniv.nl/WISH/>), and we discuss these lines first.

TABLE 1  
INTEGRATED INTENSITIES  $I = \int T_{\text{MB}} dv [\text{MK km s}^{-1}]^a$

Trans.	Freq. [Hz]	Turbulent velocity $\delta v$ [ $\text{km s}^{-1}$ ] <sup>b</sup>					
		No freeze-out		$x_f = 10^{-8}$		$x_f = 10^{-10}$	
		0.5	2.0	0.5	2.0	0.5	2.0
ortho- $\text{H}_2\text{O}$ lines							
$1_{10}-1_{01}$	556.936	13.7	66.2	16.3	59.3	13.6	41.8
$3_{12}-3_{03}$	1097.37	32.7	120.9	19.1	50.6	3.9	7.0
$3_{12}-2_{21}$	1153.13	33.5	103.6	12.5	29.0	1.4	1.9
$3_{21}-3_{12}$	1162.91	27.6	94.6	12.9	32.5	2.4	4.3
$2_{21}-2_{12}$	1661.01	34.3	143.7	29.8	97.2	10.9	20.5
$2_{12}-1_{01}$	1669.90	21.1	114.2	26.6	97.0	25.5	85.5
$3_{03}-2_{12}$	1716.77	38.9	150.2	32.3	110.1	15.5	33.2
$3_{30}-3_{21}$	2196.35	25.3	98.1	11.5	27.9	2.1	3.5
$4_{14}-3_{03}$	2640.47	28.6	125.3	25.3	73.0	9.2	20.0
$2_{12}-1_{10}$	2773.97	16.1	96.2	21.4	69.1	17.0	51.0
para- $\text{H}_2\text{O}$ lines							
$2_{11}-2_{02}$	752.029	27.6	108.7	21.3	62.5	4.9	7.9
$2_{02}-1_{11}$	987.924	39.9	138.9	29.8	102.4	10.6	17.3
$1_{11}-0_{00}$	1113.34	21.4	105.5	24.9	94.5	23.1	70.0
$2_{20}-2_{11}$	1228.80	32.7	124.5	20.7	56.9	3.9	6.0

<sup>a</sup>Adopting distance  $d = 140$  pc

<sup>b</sup> $\delta v$  is the  $1/e$  half width of line profile.

### 3.1. The $1_{10} - 1_{01}$ and $1_{11} - 0_{00}$ $\text{H}_2\text{O}$ lines

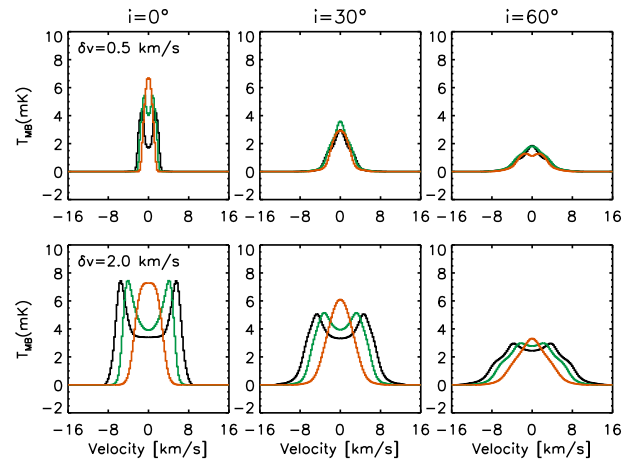


FIG. 2.— The  $1_{10} - 1_{01}$  ortho- $\text{H}_2\text{O}$  lines with the d'Alessio opacities for inclinations of  $0^\circ$  (left),  $30^\circ$  (middle), and  $60^\circ$  (right); no freeze-out (black), with freeze-out below 110 K and abundance  $x_f(\text{H}_2\text{O}) = 10^{-8}$  (green) and  $x_f(\text{H}_2\text{O}) = 10^{-10}$  (red) in the freeze-out zone; turbulent velocity  $\delta v = 0.5$  (top), and  $2.0 \text{ km s}^{-1}$  (bottom).

The line profiles of the 556.936 GHz  $1_{10} - 1_{01}$  ortho and the 1113.34 GHz  $1_{11} - 0_{00}$  para transitions are convolved with the  $38''$  and  $19''$  *Herschel* beam sizes at these frequencies. Fig. 2 shows how the profile of the  $1_{10} - 1_{01}$  ortho transition is affected by changes in inclination angle  $i$ , turbulent velocity  $\delta v$ , and the effects of incomplete freeze-out. Variations in  $i$  are shown horizontally across the figure, and changes in  $\delta v$  vertically; the three lines represent no freeze-out and freeze-out that leaves residual water abundances of  $10^{-8}$  and  $10^{-10}$ . The integrated intensities for the models shown vary between 14 and 66  $\text{mK km s}^{-1}$ , and are mainly sensitive to the line width. The  $1_{10} - 1_{01}$  ortho- and  $1_{11} - 0_{00}$  para- $\text{H}_2\text{O}$  lines have similar integrated intensities, with line ratios  $1_{10} - 1_{01}/1_{11} - 0_{00} \sim 0.6$ . The small variations in this ratio, caused by high opacities in the lines, makes these lines unfavorable as diagnostics.

Due to the rotation of the disk, the lines are broadened with increasing inclination, but at increasingly smaller integrated intensities because of the reduction of the apparent surface area of the disk. For a completely edge on disk, absorption by the cold outer regions ( $R \gtrsim 100$  AU) is important, but this effect has not been included in the present calculations. At an inclination of  $60^\circ$ , the rotational broadening extends to  $5 \text{ km s}^{-1}$  (best seen at  $\delta v = 0.5 \text{ km s}^{-1}$ ), which corresponds to a rotational velocity of  $v_r = 10 \text{ km s}^{-1}$  or a radius of  $R = 10$  AU. The dominant contributions to the  $1_{10} - 1_{01}$  line flux originate therefore from  $R \gtrsim 10$  to 100 AU. Thus this line provides no information on the snow line, which is located close to the star, near  $R \sim 1$  AU in this model (see Fig. 1).

At an inclination  $i = 0^\circ$  (face-on disk), the line width is determined by the turbulent velocity  $\delta v$  and the line opacity. The center of the line is strongly self-absorbed for no freeze-out, since the emission produced at  $N_{\text{H}} \sim 10^{22} - 10^{23} \text{ cm}^{-2}$  is absorbed by the upper layers. These regions are sub-thermally excited because the densities are low ( $n_{\text{H}} < 10^8 \text{ cm}^{-3}$ ). Self-absorption occurs, but

to a lesser extent, when freeze-out is included and the residual water vapor abundance is  $x_f(\text{H}_2\text{O})=10^{-8}$ . Even for  $x_f(\text{H}_2\text{O})=10^{-10}$ , the line is still optically thick. For finite inclination angles,  $i = 30^\circ$  and  $60^\circ$ , flux loss at line center can also occur for the freeze-out model with a water vapor abundance  $x_f(\text{H}_2\text{O}) = 10^{-10}$ . This is most clearly seen for the case  $\delta v = 0.5 \text{ km s}^{-1}$ . This is not a signature of the snow line, since the flux loss occurs for  $i = 60^\circ$ , for example, for velocities  $v < 2 \text{ km s}^{-1}$ , corresponding to radii  $R > 50 \text{ AU}$ .

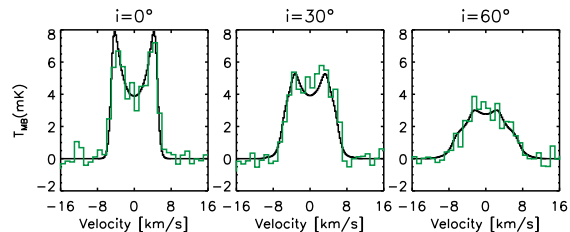


FIG. 3.— The  $1_{10} - 1_{01}$  ortho- $\text{H}_2\text{O}$  line profile with a turbulent velocity of  $2.0 \text{ km s}^{-1}$  for inclinations (from left to right)  $i = 0^\circ$ ,  $30^\circ$ ,  $60^\circ$ , with freeze-out and  $x_f(\text{H}_2\text{O}) = 10^{-8}$ . The model results are in black. For the curves in green, a  $1\sigma$  noise level of  $0.5 \text{ mK}$  has been added. The velocity resolution is assumed to be  $1 \text{ km s}^{-1}$ .

In Fig. 3, we test how well the shape of the  $1_{10} - 1_{01}$  line can be measured by *Herschel*. The model is shown in black, and a  $1\sigma$  noise level of  $0.5 \text{ mK}$  has been added in green. The sensitivity of the *Herschel* detectors at  $1113.34 \text{ GHz}$  is about four times less than at  $556.936 \text{ GHz}$ . According to the time estimator for the *Herschel* Space Observatory (<http://www.esac.esa.int>), a  $1\sigma$  noise level of  $0.5$  and  $2.0 \text{ mK}$  can be obtained at the frequencies of the  $1_{10} - 1_{01}$  ortho and  $1_{11} - 0_{00}$  para transition, respectively, in about 4 hours of observing time, when frequency switching is used and a spectral resolution of  $1 \text{ km s}^{-1}$  is requested. Thus one should be able to determine the width, and to some degree the shape of the  $1_{10} - 1_{01}$  ortho- $\text{H}_2\text{O}$  line. However, the effect of self-absorption due to high opacities will be hard to distinguish for low turbulent velocities ( $\delta v \leq 1.0 \text{ km s}^{-1}$ ) at this resolution. The para line is not a good candidate as the ortho transition for obtaining a line shape at the same noise level because of the decrease in sensitivity.

### 3.2. Line ratios

The line profiles and integrated intensities of the  $1_{10} - 1_{01}$  and its ratio with the  $1_{11} - 0_{00}$  transition are affected by inclination angle, turbulent broadening, and the residual water vapor abundance after freeze-out. The dust opacity, which is influenced by grain growth and settling, can also play a role, although our study of these effects indicates that this is less important than the variables just mentioned. Thus the models are degenerate in the sense that different parameter sets give the same line shapes and intensities, due to the high opacities in these lines. Unfortunately, these are the only lines to be observed in the WISH program. Observing higher excitation transitions would help, but the decrease in sensitivity with frequency means that only line fluxes and not line shapes can be determined by *Herschel* observations. At a velocity resolution of  $1 \text{ km s}^{-1}$ , it would take *Herschel* about 4 hours to get the  $1\sigma$  noise level down to

$2 \text{ mK}$  for transition frequencies around  $\sim 1100 \text{ GHz}$ . In a similar observation around  $\sim 1700 \text{ GHz}$ , the noise level would be  $8 \text{ mK}$ .

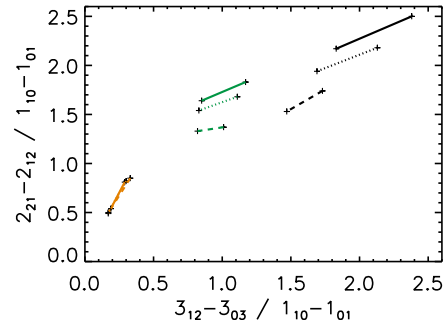


FIG. 4.— The  $3_{12} - 3_{03}/1_{10} - 1_{01}$  versus the  $2_{21} - 2_{12}/1_{10} - 1_{01}$  ratio for models without freeze-out (black), models with gas-phase abundances in the freeze-out zone of  $x_f(\text{H}_2\text{O}) = 10^{-8}$  (green) and  $10^{-10}$  (orange). The different lines are for inclinations  $i = 0^\circ$  (solid),  $30^\circ$  (dotted), and  $60^\circ$  (dashed).

Inspection of Table 1 shows that higher transitions may be observable with *Herschel*. We will now focus on the  $3_{12} - 3_{03}$  transition at  $1097.37 \text{ GHz}$  and the  $2_{21} - 2_{12}$  transition at  $1661.01 \text{ GHz}$ , although other lines may also have diagnostic value. Fig. 4 plots the ratios of these two lines to the fundamental  $1_{10} - 1_{01}$  transition, and shows that the ratios can distinguish between different levels of water vapor in the freeze-out zone. The model results for no freeze-out are found in the right upper part of the figure, where there are three segments for inclination  $i = 0^\circ$ ,  $30^\circ$  and  $60^\circ$ ; each segment consists of two values of the turbulent velocity,  $\delta v = 0.5$  and  $2.0 \text{ km s}^{-1}$ . Similar sets for  $x_f = 10^{-8}$  (middle part) and  $x_f = 10^{-10}$  (left lower part) are clearly in a different part of the diagram and do not overlap with each other. The variations due to inclination and turbulent velocity are smaller than those associated with freeze-out.

## 4. CONCLUSIONS

We have shown that it should be possible to observe some far-infrared rotational lines of water with the HIFI instrument on *Herschel* that are produced in regions between radii  $R \sim 10 - 100 \text{ AU}$ . The current scheduled observations of the  $1_{10} - 1_{01}$  and  $1_{11} - 0_{00}$  transitions would provide information on the spatial distribution of water and on turbulence if the inclination of the disk is known. The ratios of these lines are quite similar for the different models ( $\sim 0.9 - 1.0$ ), which is due to the high opacities in both lines. The line shapes of the  $1_{10} - 1_{01}$  transition for different water vapor residuals in the freeze-out zone are quite similar at the same inclination angle. When measurements of the  $1_{10} - 1_{01}$  line are combined with higher transitions, such as the  $3_{12} - 3_{03}$ , and  $2_{21} - 2_{12}$  lines, the abundance of the residual water vapor in the freeze-out zone can be determined (see Fig. 4). These *Herschel* observations of rotational lines will complement observations of shorter-wavelength excitation lines by *Spitzer* ( $10\text{-}20\mu\text{m}$ , e.g., Carr & Najita 2008; Salyk et al. 2008), *SOFIA* ( $6\mu\text{m}$ ), and near-infrared ro-vibrational transitions (Carr et al. 2004; Salyk et al. 2008)). These lines trace the inner regions of the disk

out to radii  $R \sim 1 - 2$  AU, with the potential of providing information on the conditions in the immediate neighborhood of the snow line.

#### 5. ACKNOWLEDGEMENTS

This work has been supported by NSF Grant AST-0507423 and NASA Grant NNG06GF88G to UC Berke-

ley. We would like to express our appreciation to Dr. Floris van der Tak for providing the 2D version of SKY, and to Dr. Paola d'Alessio for providing the dust opacities. We would also like to thank the referee for the comments about the dust opacities.

#### REFERENCES

- Boonman, A. M. S., Doty, S. D., van Dishoeck, E. F., et al. 2003, *A&A*, 406, 937
- Carr, J. S. & Najita, J. R. 2008, *Science*, 319, 1504
- Carr, J. S., Tokunaga, A. T., & Najita, J. 2004, *ApJ*, 603, 213
- D'Alessio, P., Calvet, N., & Hartmann, L. 2001, *ApJ*, 553, 321
- D'Alessio, P., Calvet, N., Hartmann, L., Lizano, S., & Cantó, J. 1999, *ApJ*, 527, 893
- Davis, S. S. 2007, *ApJ*, 660, 1580
- Dullemond, C. P., Hollenbach, D., Kamp, I., & D'Alessio, P. 2007, in *Protostars and Planets V*, ed. B. Reipurth, D. Jewitt, & K. Keil, 555–572
- Faure, A. & Josselin, E. 2008, *A&A*, submitted
- Fraser, H. J., Collings, M. P., McCoustra, M. R. S., & Williams, D. A. 2001, *MNRAS*, 327, 1165
- Garaud, P. & Lin, D. N. C. 2007, *ApJ*, 654, 606
- Glassgold, A. E., Najita, J., & Igea, J. 2004, *ApJ*, 615, 972
- Hayashi, C. 1981, *Progress of Theoretical Physics Supplement*, 70, 35
- Hogerheijde, M. R. & van der Tak, F. F. S. 2000, *A&A*, 362, 697
- Jonkheid, B., Dullemond, C. P., Hogerheijde, M. R., & van Dishoeck, E. F. 2007, *A&A*, 463, 203
- Jonkheid, B., Faas, F. G. A., van Zadelhoff, G.-J., & van Dishoeck, E. F. 2004, *A&A*, 428, 511
- Kamp, I. & Dullemond, C. P. 2004, *ApJ*, 615, 991
- Lecar, M., Podolak, M., Sasselov, D., & Chiang, E. 2006, *ApJ*, 640, 1115
- Meijerink, R., Glassgold, A. E., & Najita, J. R. 2008, *ApJ*, 676, 518
- Nomura, H., Aikawa, Y., Tsujimoto, M., Nakagawa, Y., & Millar, T. J. 2007, *ApJ*, 661, 334
- Podolak, M. & Zucker, S. 2004, *Meteoritics and Planetary Science*, 39, 1859
- Poelman, D. R. & Spaans, M. 2005, *A&A*, 440, 559
- Poelman, D. R. & Spaans, M. 2006, *A&A*, 453, 615
- Salyk, C., Pontoppidan, K. M., Blake, G. A., et al. 2008, *ApJ*, 676, L49
- Sasselov, D. D. & Lecar, M. 2000, *ApJ*, 528, 995
- Schöier, F. L., van der Tak, F. F. S., van Dishoeck, E. F., & Black, J. H. 2005, *A&A*, 432, 369
- Thi, W.-F. & Bik, A. 2005, *A&A*, 438, 557